Macromolecules

Article

pubs.acs.org/Macromolecules

Composites of Functional Poly(phenylacetylene)s and Single-Walled Carbon Nanotubes: Preparation, Dispersion, and Near Infrared Photoresponsive Properties

Xiao-Qing Liu,[†] Yi-Lun Li,[‡] Yuan-Wei Lin,[§] Shuang Yang,[†] Xue-Feng Guo,[§] Yan Li,[‡] Juan Yang,*[,‡] and Er-Qiang Chen*[,†]

[†]Beijing National Laboratory for Molecular Sciences, Department of Polymer Science and Engineering and the Key Laboratory of Polymer Chemistry and Physics of Ministry of Education, College of Chemistry and Molecular Engineering, Peking University, Beijing 100871, China

[‡]Beijing National Laboratory for Molecular Sciences, State Key Laboratory of Rare Earth Materials Chemistry and Applications, Key Laboratory for the Physics and Chemistry of Nanodevices, College of Chemistry and Molecular Engineering, Peking University, Beijing 100871, China

[§]Beijing National Laboratory for Molecular Sciences, State Key Laboratory for Structural Chemistry of Unstable and Stable Species, College of Chemistry and Molecular Engineering, Peking University, Beijing 100871, China

Supporting Information

ABSTRACT: To explore poly(phenylacetylene) (PPA) derivatives as the dispersing agent of single-walled carbon nanotubes (SWNTs), we synthesized a new series of side chain PPAs (denoted as PPA-*m*, *m* = 2, 1, 0). The side chains of PPA-*m* bear a soluble 3,4,5-tris(octyloxy)phenyl moiety at the end, and a biphenyl (*m* = 2), a phenyl (*m* = 1), or no phenyl ring (*m* = 0) in the middle linked to the PPA main-chain through an ether linkage. All the three PPA-*m*s can efficiently disperse SWNTs in organic solvents forming stable SWNTs/PPA-*m* composites. The composites were characterized by microscopy method, absorbance and photoluminescence spectroscopy. Quantitative analysis shows that there is a tendency for PPA-*m* to preferentially disperse SWNTs with large diameters in tetrahydrofuran and toluene when compared with the normally used surfactant of sodium dodecyl sulfate. The effective interactions between PPA-*m* and SWNTs should be ascribed to the helical wrapping of the PPA-*m* backbone on SWNTs and the $\pi-\pi$ interactions between the phenyl groups and SWNTs. The long alkyl tails on the side-chains also prevent individual SWNTs from reaggregation. Additionally, the near-infrared (nIR) photoresponsive electrical conductivity of the SWNTs/PPA-2 composite is measured, indicating a 12% increase of the photocurrent upon the nIR irradiation, which is greater compared with that of the reported pure SWNTs film.

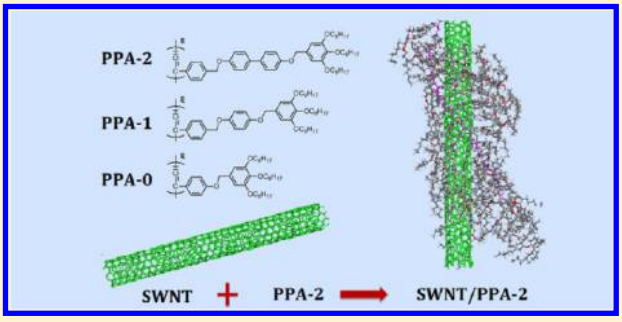

INTRODUCTION

Polymer composites of single-walled carbon nanotubes (SWNTs) have stimulated a great deal of interest due to their promising application in advanced materials,[1−3] including mechanical reinforcing materials,[4−6] flexible electronics,[7−9] sensors,[10−12] and photovoltaic devices.[13,14] In particular, researches have focused on obtaining the maximum benefits from SWNTs in polymer composites.[15] The unique electronic and optical properties of SWNTs are determined by their chiral index (*n*,*m*), which defines the tube diameter, chiral angle, and metallic or semiconducting character.[16] Current bulk synthesis methods of SWNTs, however, produce mixtures of nanotubes with different diameters and chiralities owning various electronic band structures. Therefore, it is desirable to purify SWNT samples to get high purity of single-species SWNT. A great challenge is that SWNTs tend to aggregate into bundles due to the strong $\pi-\pi$ interaction between the sp^2 sidewalls,[17] which significantly reduces the dispersion degree and compatibility in the composite systems, and further strongly affects the fabrication of SWNTs/polymer composites toward high-performance devices.

The noncovalent functionalization of SWNTs by conjugated polymers has emerged as an attractive method to approach the problems mentioned.[15,18] Conjugated polymers with extensive π-conjugated backbone can interact with the sidewalls of SWNTs through $\pi-\pi$ interactions. For example, poly(*m*-phenylenevinylene)s, the backbone of which tends to take a helical conformation wrapping around SWNTs, have been known as a good dispersing agent for SWNTs.[19,20] Poly(*p*-phenyleneethynylene)s, however, owing to their linear rigid backbones, cannot wrap around the nanotubes but can interact with the SWNT surface by $\pi-\pi$ stacking.[21] It is further found

Received: August 6, 2013
Revised: October 5, 2013
Published: October 21, 2013

   dx.doi.org/10.1021/ma401647a | *Macromolecules* 2013, 46, 8479−8487

that several other conjugated polymers can form stable complex with SWNTs, such as polythiophenes[22,23] and polyfluorenes,[24] which in turn favors for the exciton dissociation[25] and energy transfer.[26] In addition, conjugated polymers have also been used to purify SWNT mixture of various species.[18] Polyfluorenes and polycarbazoles have been reported to show special selectivity to dispersing several semiconducting species while excluding metallic ones,[27−30] providing a potential route toward the bulk separation of metallic and semiconducting SWNTs.

Polyacetylene (PA) is the prototype conjugated polymer and can be easily derivatized by introducing various functional groups on the side chains, which have demonstrated unique functions in the fields of electronic, optical, liquid crystalline, and biological materials.[31,32] Compared with the conjugated polymers mentioned above, however, PAs received less attention as dispersing agents for SWNTs. Tang et al. have reported the poly(phenylacetylene)s (PPA) composites of carbon nanotubes (CNTs) prepared by in situ polymerization[33] or by noncovalent wrapping process.[34] The CNTs/PPAs hybrids show efficient charge transfer[35,36] and superparamagnetic[37] properties, and good biocompatibility.[34] On the basis of delicate design of the PPAs chemical structures, their work has proved that functional PPAs have strong dispersing power toward CNTs in different solvents, including water. In particular, they have revealed that wrapping with polymer backbone,[38] $\pi-\pi$ interactions and donor−acceptor interactions[35] between aromatic pendants and CNTs are three important factors that affect the dispersion ability. Specially, their research concentrated mainly on PPAs composites of multiwalled carbon nanotubes (MWNTs). However, with regard to SWNTs, to disperse SWNTs efficiently using PPAs as dispersing agents remains a challenge. The achievement on MWNTs/PPAs composites stimulates us to explore PPAs composites with SWNTs, which are expected to show extraordinary optoelectronic properties.

In the present work, inspired by Tang's study, we design a new series of PPA derivatives, denoted as PPA-*m* (m = 2, 1, 0), of which the chemical structures are shown in Scheme 1. From the view of chemical structure, introducing aromatic group onto the side chain of PPA derivatives may increase the strength of polymer binding to the nanotube sidewall, which will aid the fabrication of PPAs composites with SWNTs. Therefore, for the three polymers synthesized, biphenyl, phenyl ring, or no phenyl is attached to the PPA backbone through an ether linkage (represented by the m = 2, 1, or 0 in the samples' abbreviations), respectively. The effect of varying side chains of PPAs on the interaction between polymers and nanotubes was investigated. To further improve the solubility of the polymers, a 3,4,5-tris(octyloxy)phenyl moiety, which contains three octyl tails, is used as the end group of the side chain. All of these PPAs can efficiently disperse SWNTs in organic solvents and show a tendency to preferentially disperse SWNTs with large diameters when compared with the normally used surfactant of sodium dodecyl sulfate (SDS). As a tentative study, the nIR photoresponsive electrical conductivity of the SWNTs/PPA-2 composite was measured. An enhanced photoconductivity of the composite film compared with that of the reported pure SWNTs film is observed, making them an attractive kind of polymer composites with SWNTs.

Scheme 1. Chemical Structures of the Synthesized PPA-*m* (m = 2, 1, 0)

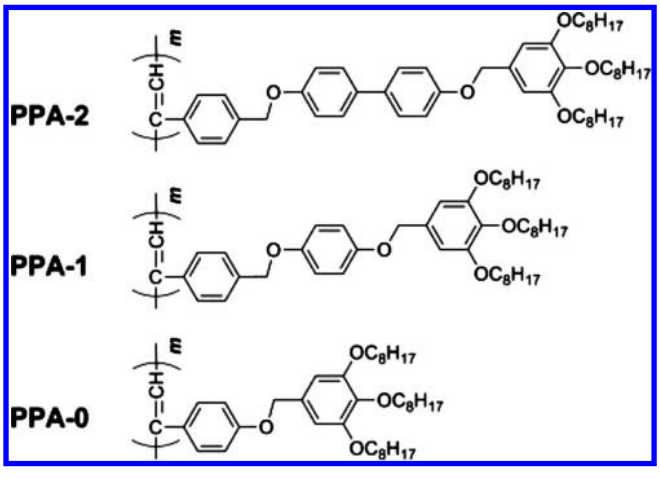

RESULTS AND DISCUSSION

Synthesis of Monomers and Polymers. Scheme 2 gives the synthesis route of the monomers and polymers. The details of synthesis and characterization of the compounds and polymers are provided in the Supporting Information. First, a 3,4,5-tris(octyloxy)phenyl moiety was prepared via Williamson ether synthesis with *n*-octyl bromide and methyl-3,4,5-tris(hydroxy)benzoate, followed by reduction to the benzyl alcohol and chlorination to the benzyl chloride (3C8-Cl).[39] To introduce biphenyl and phenyl groups into the monomers MA-2 and MA-1, 2,2′-biphenol and hydroquinone were reacted with 4-bromobenzyl bromide to get the compounds HO-biph-Br and HO-ph-Br, respectively. The phenolic hydroxy groups were used to react with 3C8-Cl, while the 4-bromo group was further converted to the alkynyl by Sonogashira reaction and deprotection of the trimethylsilyl.[40] As a comparison, MA-0 was obtained with no phenyl ring between the phenylacetylene and the soluble moiety, and thus the corresponding polymer owns the smallest side chain.

Polymerizations of the monomers were carried out under mild condition using $[Rh(nbd)Cl]_2$ as the catalyst.[41] Yellow solids were obtained for the polymers with excellent yield except PPA-0 (Table 1). The relative low yield of PPA-0 may be attributed to the electron-richer $-OCH_2$ group at *para* position of the phenylacetylene group.[42] The molecular weights of PPA-*m*s were determined using gel permeation chromatography (GPC) relative to polystyrene standards. With the highest polymerization yield, the number-average molecular weight (M_n) of PPA-2 is 107 kDa, larger than those of PPA-1 and PPA-0, 99 kDa and 64 kDa, respectively. Owning to the soluble moiety at the end of the side chains, all the polymers dissolved well in the common solvents, such as tetrahydrofuran (THF), toluene, dichloromethane, and chloroform.

The chemical structures of PPA-*m*s were confirmed by ^{1}H NMR spectroscopy. Figure 1 compares the ^{1}H NMR result of PPA-2 with that of MA-2. The signal at 3.08 ppm is attributed to the acetylene proton in MA-2, which disappeared after polymerization. A new peak associated with the olefinic proton in PPA-2 can be observed at 5.97 ppm, indicating a *cis*-rich conformation of the main-chain.[43,44] The ^{1}H NMR spectra of PPA-1 and PPA-0 are also included in Figure 1, of which the corresponding olefinic protons appear at 5.87 and 5.82 ppm, respectively.

Polymer Composites of SWNTs/PPA-*m*. Composites of PPA-*m* with SWNTs were prepared by solution mixing. In a

dx.doi.org/10.1021/ma401647a | Macromolecules 2013, 46, 8479−8487

Scheme 2. Synthesis Route of the Monomers and Polymers

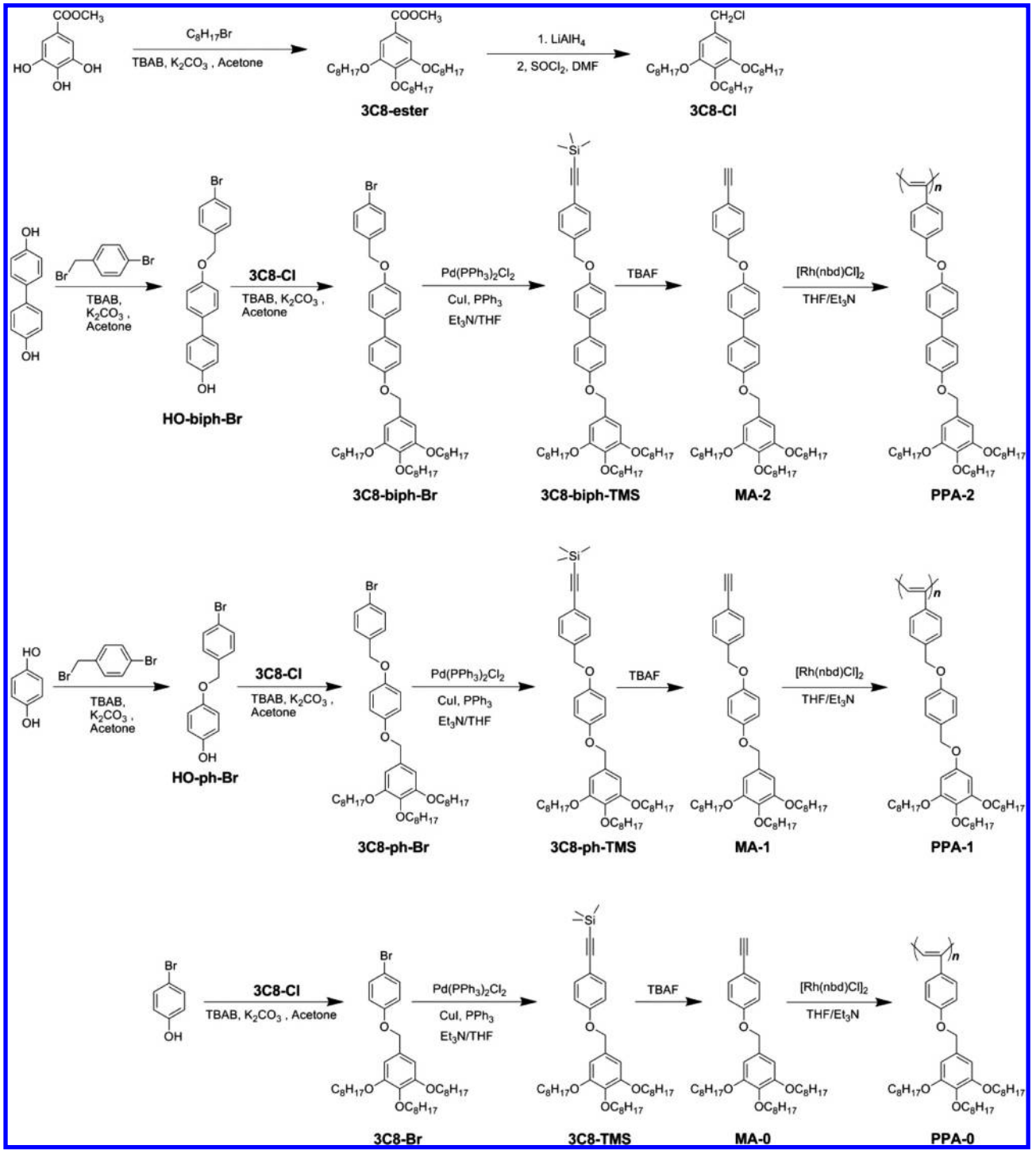

Table 1. Polymerization Results of PPA-*m* (*m* = 2, 1, 0)

polymer	yield (%)[a]	M_n (kDa)[b]	M_w (kDa)[b]	PDI[b]
PPA-2	86.9	107	213	2.0
PPA-1	70.0	99	185	1.9
PPA-0	53.0	64	147	2.3

[a]Polymerization carried out in THF using $[Rh(nbd)Cl]_2$ as the catalyst at 30 °C under nitrogen for 24 h; [monomer] = 0.2 M, [catalyst] = 2 mM. [b]Estimated by GPC in THF on the basis of a polystyrene calibration.

typical experiment, a certain amount of SWNTs (CoMoCAT, 0.20 mg) was added to the solution of PPA-*m* in THF (5.00 mg/5.00 mL). The mixture was sonicated with a tip sonicator for 30 min at 0 °C, followed by ultracentrifuging at 100000*g* for 30 min. It should be mentioned that the ultracentrifugation process helps to remove the carbon impurities and SWNT bundles to some degree. We chose the centrifugation force of 100000*g* out of the consideration for spectroscopy characterization (see Figure S1 in Supporting Information). The resulting supernatant was carefully transferred to obtain the stable SWNTs/PPAs composite solution. All the PPA-*m*s

dx.doi.org/10.1021/ma401647a | *Macromolecules* 2013, 46, 8479−8487

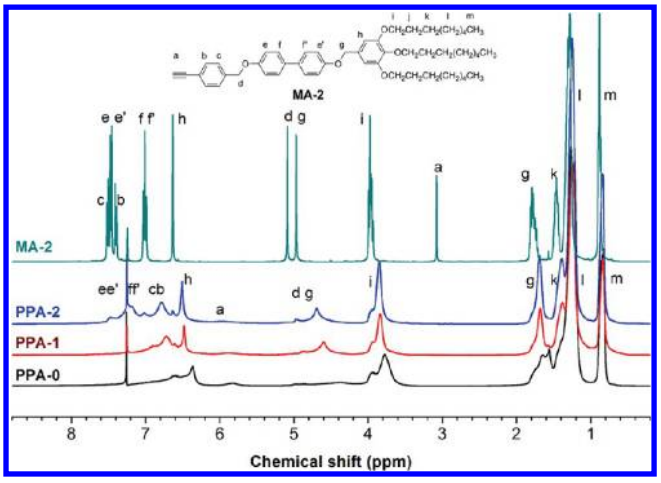

Figure 1. ^{1}H NMR spectra of the monomer MA-2 and the polymers PPA-2, PPA-1, and PPA-0 in $CDCl_3$.

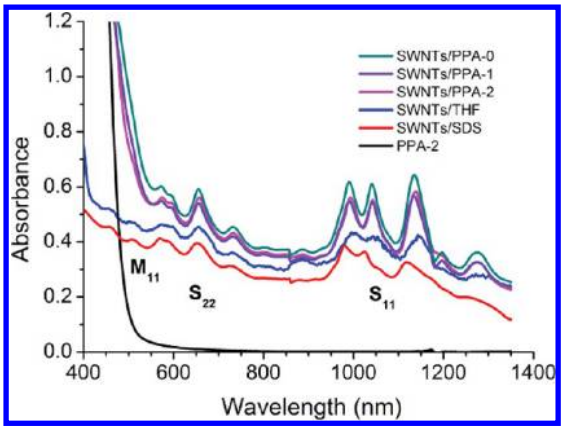

Figure 3. UV−vis-nIR absorbance spectra of dispersed SWNTs in THF solutions of PPA-*m* (1 mg/mL) and in aqueous SDS solution (1 wt %). Note that due to the poor dispersion ability of SWNTs in THF, the absorption of SWNTs/THF (blue line) is rather weak. For clarity, the blue line in the figure is an enlarged one, corresponding to the original data of SWNTs/THF multiplied by 9.

exhibit efficient dispersion of SWNTs in THF, toluene, and chloroform, even when the initial amount of SWNTs was up to 1 mg. The resultant supernatants remained stable for periods of at least 3 months with no observable precipitation (Figure S2 in Supporting Information). A dispersion of the same batch of raw SWNTs in SDS aqueous solution was also prepared, following a published procedure.[45]

Morphology characterization of SWNTs/PPA-*m* composites was performed using transmission electron microscopy (TEM). TEM samples were prepared by simply depositing a drop of the composite solution on copper grids coated with lacey support film. Figure 2 reveals some long fibrils of polymer-coated nanotubes spanning the holes on the grid, where the contrast was enhanced for high-resolution imaging. Practically, the presence of the polymers makes TEM difficult to discern the nanotube side wall from the polymer matrix. We found, however, several regions clearly showing the presence of SWNTs. Judging from the dimension of fibril suspended on the hole shown in Figure 2, parts b and c, we consider that the fibril should contain individual SWNT. According to the TEM observation, it is evident that SWNT bundles can be efficiently exfoliated into individuals by the PPAs.

Absorbance. UV−vis−nIR absorbance measurements were taken to characterize the absorption properties of SWNTs/PPA-*m* composites (Figure 3). All the samples were prepared by dispersing 0.20 mg of SWNTs in the PPA-*m* solutions (1.00 mg/mL in 5.00 mL of THF) and ultracentrifuging at 100000*g* for measurement. For comparison, the absorption spectrum of SWNTs dispersed by SDS in H_2O was also shown. Owing to the absorption of the polyene main chain,[40] PPA-*m*s show an absorption band up to about 550 nm. This absorption background remains in the spectra of SWNTs/PPA-*m*s, and overlaps with the relatively weak absorptions ascribed to the first interband transitions of metallic SWNTs (M_{11}). Meanwhile, the absorption features that correspond to the first (S_{11}) and second (S_{22}) interband transitions for semiconducting SWNTs can be found from 800 to 1400 nm and 600 to 800 nm, respectively.[46] Compared with the absorbance of SWNTs dispersed by SDS, the absorption peaks of the SWNTs/PPAs become better resolved, suggesting that SWNTs can be more efficiently exfoliated into individuals or small bundles by PPA-*m* in THF.[47] In the cases of THF as the solvent, the absorption peaks located at 1200 to 1400 nm, which cannot be distinguished in SWNTs/SDS, are ascribed to absorptions of SWNTs with large diameters (~1 nm).[16] This indicates that THF is helpful for dispersing SWNTs of large diameters and PPA-*m* improves the dispersion degree even more. In addition, the SWNT absorption peaks (particular for S_{11} band) are found to be red-shifted by 10−30 nm in the SWNTs/PPA-*m*s relative to those in SDS aqueous solution, which has been reported previously with other conjugated polymers[28,48,49] due to the surrounding polymers causing a difference in the local dielectric

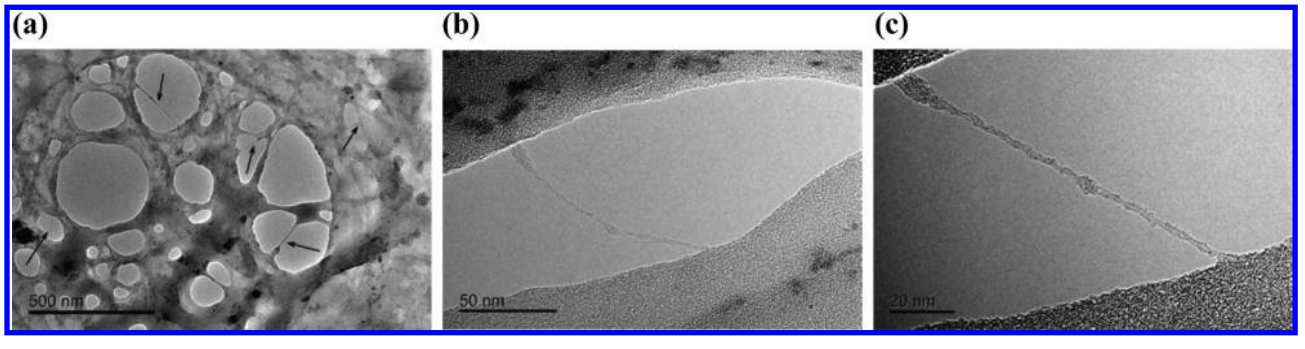

Figure 2. TEM images of SWNTs/PPA-2 composites prepared in THF at different magnifications. The black arrows in part a indicates long SWNTs/polymers fibrils spanning holes on the grid. The high-magnification images (b and c) clearly show the presence of individual polymer-wrapped SWNTs. Scale bars are 500 (a), 50 (b), and 20 nm (c).

dx.doi.org/10.1021/ma401647a | *Macromolecules* 2013, 46, 8479−8487

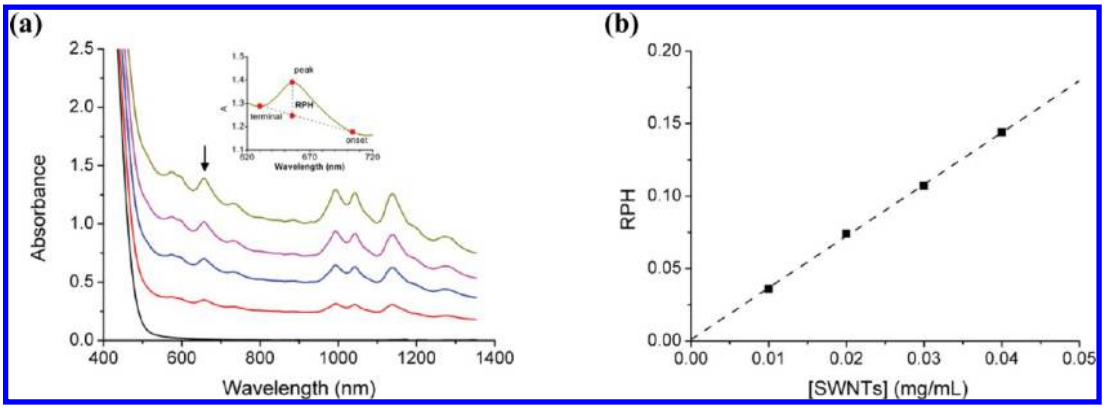

Figure 4. (a) UV−vis−nIR absorbance spectra of SWNTs/PPA-2 in THF with different SWNT concentrations (mg/mL, from lower to upper): 0.000, 0.010, 0.020, 0.030, and 0.040 mg/mL. The inset graph illustrates the estimation of RPH. (b) Calibration curve for the effective SWNT concentration in the dispersion obeying Beer's law.

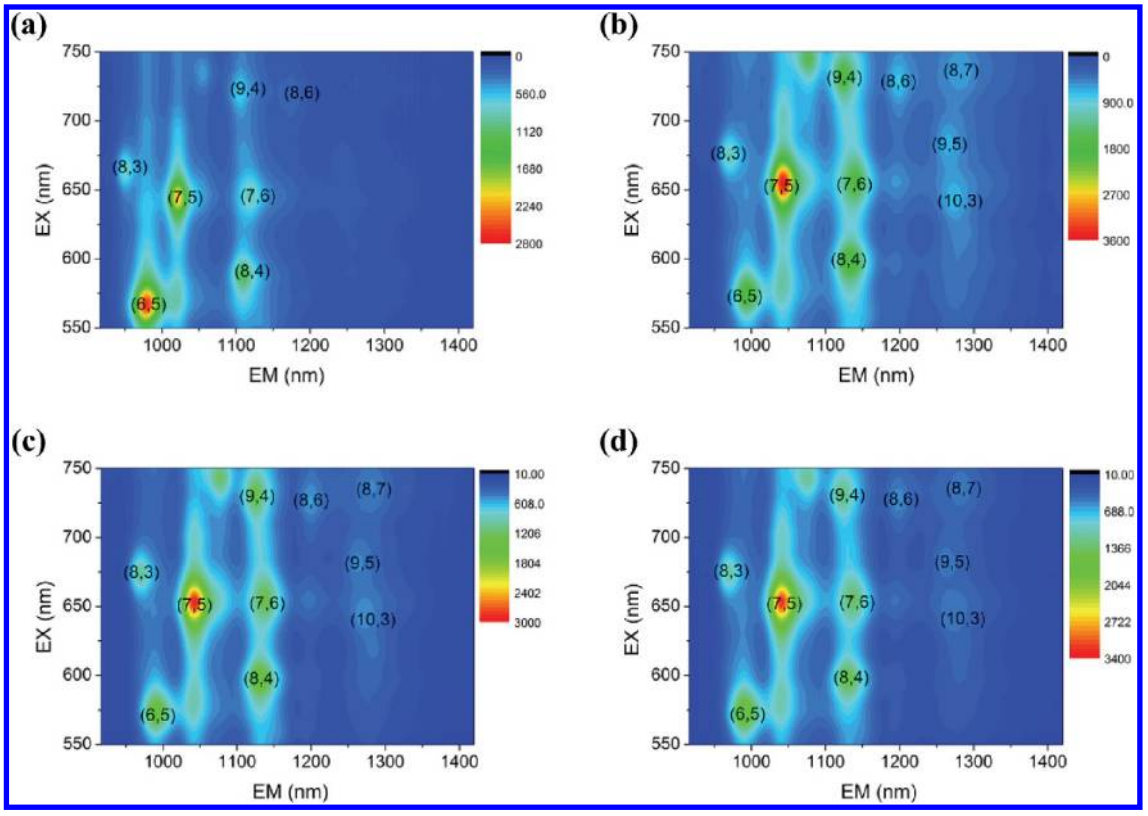

Figure 5. PLE maps of SWNTs dispersed in SDS aqueous solution (1 wt %) (a), PPA-2 (b), PPA-1 (c), and PPA-0 (d) in THF (1 mg/mL).

environment.[50,51] However, this shift is little affected by the different chemical structures of PPA-*ms* we synthesized.

According to the UV−vis−nIR spectra, we can get a view of the effective SWNT concentration in the dispersing solution. A UV−vis absorption-based approach as a direct measurement of the SWNT concentration in the supernatant has been suggested.[52,53] The concentration of SWNTs present in a sample can be directly related to the absorption corresponding to S_{22} interband electronic transitions of semiconducting SWNTs.[54] Beer's plots have been obtained to determine the unknown SWNT concentration by simply measuring the optical absorbance of the supernatant. In the present work, we also try to assess the SWNT concentration in different dispersions based on the UV−vis absorption. SWNTs/PPA-2 solutions with known SWNT concentrations were obtained by directly dispersing a certain amount of SWNTs in the PPA-2 solution (1.00 mg/mL) without ultracentrifugation. For the four measured solution samples, the known concentrations were 0.010, 0.020, 0.030, and 0.040 mg/mL, respectively. As shown in Figure 4a, broad and featureless background underneath the resonant transition peaks are attributed to the plasmon resonances of nanotubes and carbon impurities.[54] So the relative peak height (RPH)[47] with a linear background correction is used here for quantification instead of the absolute absorbance.

The estimation of RPH is illustrated by the inset graph in Figure 4a (see Supporting Information for more details of RPH). Considering that the S_{22} transition (600 to 800 nm) is less affected than the S_{11} transition, the strong peak at 656 nm was selected and monitored. The onset, peak, and termination

dx.doi.org/10.1021/ma401647a | *Macromolecules* 2013, 46, 8479−8487

wavelength are 626, 656, and 704 nm, respectively. According to Figure 4a, with increasing the SWNT concentration, the values of RPH at 656 nm were measured to be 0.036, 0.074, 0.107, and 0.143 for the four SWNTs/PPA-2 suspensions, respectively. Consequently, a linear relationship can be identified between the RPH and the SWNT concentration (Figure 4b) with a R^2 of 0.9998, conforming to Beer's law. The finding "absorptivity" value is 3.6 $(g/L)^{-1}$ cm^{-1}, in accordance with that reported by Haddon from the measurement of arc-produced SWNTs suspended in *N,N*-dimethylformamide (DMF) [35 $(mol/L)^{-1}$ cm^{-1}].[55] It is worth mentioning that, as this method has corrected the background and concerns only the relative height of the peak, it should also be suitable for the cases of centrifugated samples, in which the background absorption was reduced remarkably due to partial removal of the impurities by centrifugation (Figure S1, Supporting Information). In the following, the effective concentrations of SWNTs in the centrifugated supernatants were determined by this method.

We evaluated the dispersion ability (toward SWNTs) of PPA-2 with various concentrations. The dispersion procedure was carried out for PPA-2 in THF with polymer concentrations of 0.10, 0.50, and 1.00 mg/mL, keeping the initial SWNTs addition amount at 0.040 mg/mL. Stable SWNTs/PPA-2 composite solutions can be obtained for all three samples. The UV−vis-nIR spectra demonstrated that the absorption intensity rises with increasing PPA-2 concentration (Figure S3 in Supporting Information), suggesting that higher dispersion of SWNTs can be achieved by using more PPA-2 in solution. The accordingly determined SWNT concentrations are 0.022, 0.028, and 0.030 mg/mL, respectively, with a more significant increase when the concentrations of PPA-2 are changed from 0.10 to 0.50 mg/mL. It is noted that even the PPA-2 solution of 0.10 mg/mL demonstrates a relative high dispersion amount (0.022 mg/mL SWNTs), superior to the value of 0.013 mg/mL SWNTs by SDS of 1 wt %, further confirming the efficient dispersion of SWNTs by PPA-*m*. We conclude that PPA-*m* is the suitable candidate for preparing SWNTs/polymer composites.

Photoluminescence. Photoluminescence excitation (PLE) spectroscopy has been used to verify the effective exfoliation of SWNT bundles into individuals.[16,28,45] As the metallic tubes provide nonradiative decay pathways for photoexcited carries in the bundle, the photoluminescence (PL) efficiency of the samples demonstrates a direct relationship to the degree of debundling of semiconducting SWNTs. Figure 5 shows PLE maps of SWNTs/SDS and SWNTs/PPA-*m*. Each peak can be assigned with a specific (n,m) index according to their excitation and emission wavelengths.[16] It is found that in the SWNTs/PPA-*m* map the peaks are red-shifted relative to those in the SWNTs/SDS map, which agrees well with the red-shift observed in the UV−vis-nIR spectra. The most distinguished difference between the maps lies in the enhanced intensity of several peaks for SWNTs/PPA-*m*, especially for the SWNT species of (10,3), (8,6), (9,5), and (8,7). It is generally thought that SDS has no dispersion selectivity toward SWNTs, so the changes of peak intensities indicate that the distribution of SWNTs species in the composite is strongly affected by PPA-*m*.

To quantify such an altered distribution, we first estimated the relative content for each (n,m) semiconducting SWNT in the supernatant from its PLE map.[27] According to Y. Oyama's theoretical calculation of the PL intensity of SWNTs with different chiralities, the experimentally observed PL intensity of the SWNT with a specific (n,m) can be regarded as a product of the theoretical PL intensity and its amount in the disperse solution.[56] Thus, we obtained the relative population of the identified semiconducting species through dividing the experimental PL intensity by the theoretical PL intensity. Table 2 shows the calculated relative content of each (n,m) SWNT in different disperse solutions. According to the results measured from the SDS aqueous solution, SWNTs with diameters less than 0.9 nm dominate the as-produced SWNTs sample, in which (6,5) SWNT is the most abundant. Such a distribution has been significantly changed when PPA-*m* is used as the dispersing agent. Taking PPA-2 as an example, (7,5) SWNT becomes the dominant, and the abundances for SWNTs with larger diameters increase with nearly double percentages for (9,5) and (8,7) species in comparison with those measured from the SDS aqueous solution. We also compare the content increase of SWNTs dispersed with PPA-2 relative to that with SDS in an order of increasing tube diameter (Figure 6a). An upward trend of the relative increase value can be observed with increasing SWNT diameter. When the tube diameter is less than 0.84 nm, the content increase is negative, indicating a reduced population in SWNTs/PPA-2. As the diameter increases, however, especially for (9,5) and (8,7), a positive increase means enrichment of the corresponding tube species. This contrast between SDS and PPA-2 suggests that there is a preference for PPA-2 to disperse SWNTs with larger diameters. It is worth to mention that the similar preference could also be observed when PPA-2 was used to disperse HiPco SWNTs with a wider distribution of chiralities. Typically, the contents of (9,5), (8,7), and (11,4) SWNTs (diameter ~1 nm) were enhanced in the PPA-2 solution compared with those of in SDS (See the part of dispersion of HiPco-SWNTs by PPA-2 in Supporting Information).

Table 2. Calculated Relative Content for Each (n,m) SWNT in Different Supernatants

				content (%)[d]			
(n,m)	d_t[a] (nm)	θ[b] (deg)	I_{PL}[c]	SDS	PPA-2	PPA-1	PPA-0
(6,5)	0.757	27.0	0.67	25.9	10.7	11.0	12.9
(8,3)	0.782	15.4	2.13	2.5	1.9	2.2	2.4
(7,5)	0.829	24.5	0.71	20.4	18.1	19.1	20.2
(8,4)	0.840	19.2	0.46	17.3	15.6	16.2	14.8
(7,6)	0.895	27.5	0.47	11.9	13.5	13.2	13.2
(9,4)	0.916	17.5	0.70	6.2	9.2	9.0	8.1
(10,3)	0.936	12.8	0.28	4.4	9.3	8.7	8.2
(8,6)	0.966	25.3	0.49	3.8	5.6	5.2	5.1
(9,5)	0.976	20.6	0.28	4.2	8.7	8.0	7.7
(8,7)	1.032	27.8	0.30	3.3	7.4	7.2	7.3

[a]Tube diameter of (n,m) SWNT. [b]Chiral angle of (n,m) SWNT. [c]I_{PL}: theoretical PL intensity from Oyama et al.[56] [d]Content = $(I/I_{PL})/(\Sigma_{(n,m)}I/I_{PL}) \times 100\%$, where I and I_{PL} are the observed and theoretical PL intensities of each (n,m) tube.

As shown in parts c and d of Figure 5, the PLE maps and quantification results of SWNTs/PPA-1 and SWNTs/PPA-0 bear similarity to that of SWNTs/PPA-2: the content of (6,5) SWNT is dramatically reduced while those of SWNTs with larger diameters are enhanced. The comparison with SWNTs/SDS suggests that all three PPA-*m*s demonstrate diameter preference toward larger tubes (Figure 6b). However, only slight difference can be observed among the three PPA-*m*s with regard to the "diameter tendency" (a tendency to preferentially

dx.doi.org/10.1021/ma401647a | Macromolecules 2013, 46, 8479−8487

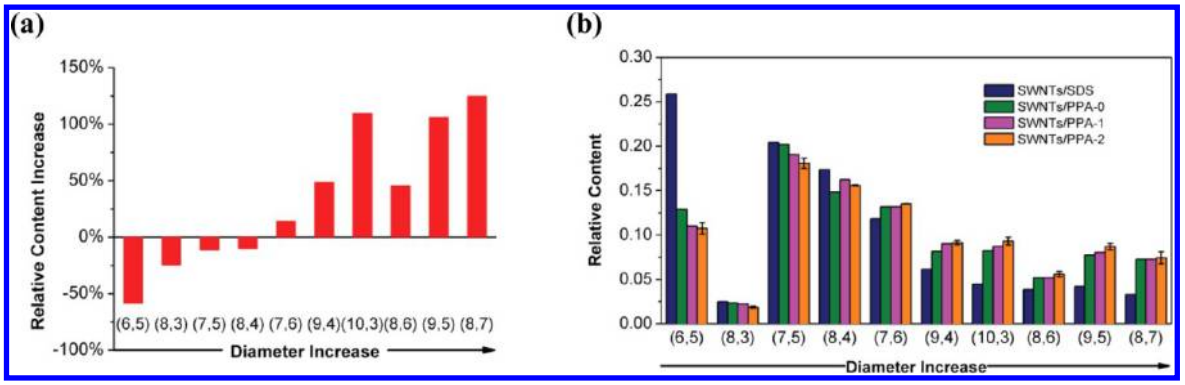

Figure 6. Relative content increase of each (*n*,*m*) SWNT dispersed by PPA-2 relative to that of SDS (a). Relative content of each (*n*,*m*) SWNT dispersed by SDS and PPA-*m*s (b).

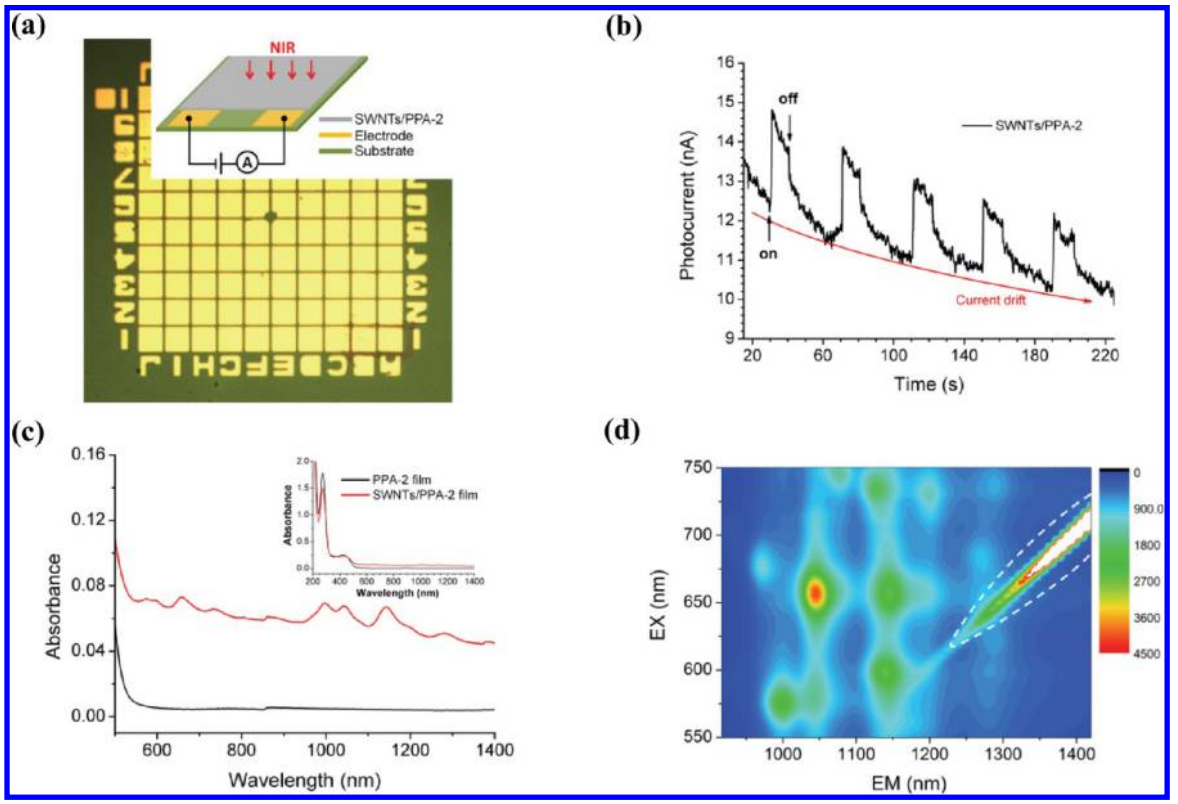

Figure 7. (a) Optical micrograph of electrodes on SiO_2/Si substrate with spinning coated SWNTs/PPA-2 film. The size of the squared metal electrode is 100 μm × 100 μm and the gap distance between every two electrodes is 10 μm. The inset brief diagram illustrates the electrical setup for the nIR photoresponse detection. (b) Photoresponsive behavior of the SWNTs/PPA-2 film (illumination power intensity: 1 mW/mm^2). The red line indicates dark current drift. (c) Absorbance spectra of the drop-casted composite film. The inset graph in part c gives the full absorption spectra of the polymer and composite film. (d) PLE map of the drop-casted composite film. The white oval encloses the double frequency emission from the exciting light in the measurement.

disperse SWNTs with larger diameters). We carried out repeated experiments of SWNTs/PPA-2 for three times, and found that the experimental error was less than 6%, as shown by the error bar in Figure 6b. Excluding the experimental error, we can infer that the "diameter tendency" of PPA-0 is slightly weaker than that of PPA-1 and PPA-2, but the "diameter tendency" of PPA-*m* is not so sensitive to the number of phenyl rings in the side-chain as we anticipated. Imin et al. have also reported that polycarbazole with different side chains do not alter the interactions between the polymers and SWNTs. The interactions with the SWNT surface are more strongly dictated by the polymer backbone than the side chain.[48] To further figure out the interactions between the polymer and SWNTs, we performed molecular dynamics simulation to search for possible conformations where PPAs surrounds a nanotube. A snapshot of the possible molecular packing scheme of PPA-2 and (7,5) SWNT is shown in Figure S7, which suggests the helical wrapping of the polymer on the tube surface, induced by strong interactions between the hydrogen of the backbone and the π-electrons of the nanotube surface.[33,57] Moreover, $\pi-\pi$ interactions occur among phenyl groups on the side chains and SWNTs with a typical interaction distance of 0.37 nm. In addition, according to the simulation result, it seems that the peripheral long alkyl chains not only partially interact with the nanotube via van der Waals interaction but also can prevent rebundling of SWNTs. As the helical wrapping may be the

dx.doi.org/10.1021/ma401647a | *Macromolecules* 2013, 46, 8479−8487

predominant factor for the effective dispersion of SWNTs, it might be reasonable that three PPA-*m*s exhibit similar dispersion ability toward SWNTs. The preference of dispersing SWNTs with large diameters cannot be well explained at this moment.

Solvents. To investigate the solvent effect, we also prepared samples of SWNTs/PPA-2 in toluene and chloroform under the condition same to that in THF (Figures S8, S9, and S10). Overall, SWNTs could be efficiently dispersed in different solvents. For the case of chloroform, due to the high density of chloroform (~1.5 g/cm^3), some big SWNT bundles suspend through buoyant forces and cannot be removed even after ultracentrifugation, causing significant fluorescence quench. Thus, the distribution of SWNTs could not be accurately acquired in chloroform solution. For the case in toluene, of which the density is similar to that of THF, the PL spectroscopy was similar to that in THF but with better resolution, suggesting the debundling efficiency in toluene is higher although the calculated SWNTs concentration from the absorbance spectra is only 0.017 mg/mL. There is obvious but irregular difference between the calculated SWNTs abundances in toluene and THF, which might be caused by the different conformation of PPA-2 induced by the difference in solvent properties, in agreement with previous reports.[49,58]

Photoresponsive Conductivity. Semiconducting SWNTs exhibit strong absorptions in the nIR region owing to their first optical transition (S_{11}), which make them promising candidates for IR detector applications.[25,59−62] The photogenerated excitons can be dissociated into free carriers thermally or by a large electric field, resulting in photocurrent generation in SWNTs.[60] And the heating of SWNTs upon nIR irradiation also reduces their resistance.[61] We investigated the nIR photoresponse in the electrical conductivity of the PPA-2 composite with SWNTs. The composite was obtained by dispersing 0.20 mg SWNTs in the PPA-2 solution of 1.0 mg/mL in 5 mL THF without centrifugation, to keep the weight ratio of SWNTs in the composite as 3.8%. The SWNTs/PPA-2 composite film were prepared by spin-casting the dispersed suspension at 800 rpm for 1 min on a silicon substrate with a 300 nm thick thermal oxide layer on top. The typical film thickness is around 50 nm determined by atomic force microscopy (AFM). Cr (8 nm)/Au (60 nm) electrodes were predeposited on the substrates using thermal evaporation, of which the optical image is shown in Figure 7a. Control samples of pure SWNTs and pure PPA-2 on the electrodes were also fabricated and characterized.

The nIR photoresponses in the composite film were observed by photoconductivity characterization. When a voltage of 10 V was applied between two electrodes, the photocurrent showed sharp rise and decay upon the on/off nIR illumination. Three features in the photoconductivity can be seen from Figure 7b. (1) The rise of the photocurrent is up to nearly 12% upon nIR illumination with the power intensity about 1 mW/mm^2. It is reported that the pure arc produced SWNT film is capable of generating a very weak photocurrent (about 0.2% increase) upon continuous-wave IR illumination (12 mW/mm^2) in the air at room temperature.[59] However, in our control experiments, no obvious photoresponse could be detected for the pure SWNTs film, which may be ascribed to the very low power intensity of nIR illumination in our case. For the pure PPA-2 film, due to its poor electrical conductivity, the photocurrent of PPA-2 cannot be characterized by the instrument we used (see Figure S11). As the current decayed immediately upon removing the irradiation as shown in Figure 7b, the current increase of 12% in SWNTs/PPA-2 cannot be explained only by sample heating. (2) The photocurrent decay is relatively slow, similar to that reported by Levitsky et al., and can be interpreted in terms of a kinetic model that takes into account the binding of photoelectrons with adsorbed oxygen.[59] For the SWNTs/PPA-2 composite, photogenerated carriers may also be captured by the coated polymers outside SWNTs, thus reducing the probability of a recombination process. (3) Current drifts can be found in periods of both light-on and light-off as depicted by the arrows in Figure 7b. In repeated experiments, both increasing and decreasing current drifts are observed, which cannot be understood for now.

The enhanced photoconductivity should be relevant to the efficient SWNTs dispersion in the composites, which has been found critical for achieving exciton dissociation.[23,25] The absorbance spectra and PLE map of a drop-casted composite film are given in Figure 7, parts c and d. The well resolved absorption and PL features evidence that no significant SWNTs aggregation recurs in the composite film, which should be attributed to the sufficient wrapping of the PPA-2 on the nanotube. The advantage of PPA-*m* in the composites deserves further investigation to improve the photoconductivity response.

■ CONCLUSION

To explore PPA derivatives as the dispersing agent of SWNTs, we have designed and synthesized a new series of side-chain PPA, namely, PPA-*m*, with a biphenyl or a phenyl or no phenyl ring attached to the PPA backbone through an ether linkage. The side-chain of PPA-*m* is ended with a soluble 3,4,5-tris(octyloxy)phenyl moiety. Owning to the effective interactions between PPA-*m* and SWNTs (helical wrapping and $\pi-\pi$ interactions), all of these PPA-*m*s can efficiently disperse SWNTs in organic solvents to form stable SWNTs/PPA-*m* composites and prevent individual SWNTs from reaggregation even in the composite film. A tendency to preferentially disperse SWNTs with larger diameters has been revealed by quantitative optical spectroscopy analysis. Our preliminary study on the nIR photoresponsive behavior of the SWNTs/PPA-2 composite film demonstrates an obvious enhanced photocurrent under nIR illumination compared with that of pure SWNTs. We are now working on further improving the photoconductivity response of the SWNTs/PPA-*m* composites.

■ ASSOCIATED CONTENT

Ⓢ Supporting Information

Materials and experimental details, characterization of the synthesized monomers and polymers, the deduction of RPH, and Figures S1−S11, showing effect of the centrifugation, pictures of the dispersion solutions, polymer concentration effect, dispersion of HiPco-SWNTs by PPA-2, molecular dynamics simulation, solvent effect, and current−voltage curves. This material is available free of charge via the Internet at http://pubs.acs.org.

■ AUTHOR INFORMATION

Corresponding Authors

*E-mail: eqchen@pku.edu.cn (E.-Q.C.).
*E-mail: yang_juan@pku.edu.cn (J.Y.).

Notes

The authors declare no competing financial interest.

■ ACKNOWLEDGMENTS

This work was supported by the National Natural Science Foundation of China (NNSFC Grants 20990232, 51273002, and 21005004), and the SRFDP of China (20100001120016).

■ REFERENCES

(1) Ajayan, P. M. *Chem. Rev.* **1999**, *99*, 1787−1799.
(2) Hu, L.; Hecht, D. S.; Grüner, G. *Chem. Rev.* **2010**, *110*, 5790−5844.
(3) Ajayan, P. M.; Tour, J. M. *Nature* **2007**, *447*, 1068−1088.
(4) Fukushima, T.; Kosaka, A.; Ishimura, Y.; Yamamoto, T.; Takigawa, T.; Ishii, N.; Aida, T. *Science* **2003**, *300*, 2072−2074.
(5) Ajayan, P. M.; Schadler, L. S.; Giannaris, C.; Rubio, A. *Adv. Mater.* **2000**, *12*, 750−753.
(6) Spitalsky, Z.; Tasis, D.; Papagelis, K.; Galiotis, C. *Prog. Polym. Sci.* **2010**, *35*, 357−401.
(7) Luo, C.; Zuo, X.; Wang, L.; Wang, E.; Song, S.; Wang, J.; Wang, J.; Fan, C.; Cao, Y. *Nano Lett.* **2008**, *8*, 4454−4458.
(8) Zou, J.; Liu, L.; Chen, H.; Khondaker, S. I.; McCullough, R. D.; Huo, Q.; Zhai, L. *Adv. Mater.* **2008**, *20*, 2055−2060.
(9) Park, H. S.; Choi, B. G.; Hong, W. H.; Jang, S. *J. Phys. Chem. C.* **2012**, *116*, 7962−7967.
(10) An, K. H.; Jeong, S. Y.; Hwang, H. R.; Lee, Y. H. *Adv. Mater.* **2004**, *16*, 1005−1009.
(11) Hangarter, C. M.; Chartuprayoon, N.; Hernández, S. C.; Choa, Y.; Myung, N. V. *Nano Today* **2013**, *8*, 39−55.
(12) Park, J.; Drahushuk, L.; Ham, M.; Kang, S. W.; Baik, J. H.; Shimizu, S.; Strano, M. S.; Song, C. *Polym. Chem.* **2013**, *4*, 290−295.
(13) Kymakis, E.; Amaratunga, G. A. J. *Appl. Phys. Lett.* **2002**, *80*, 112−114.
(14) Bounioux, C.; Katz, E. A.; Yerushalmi Rozen, R. *Polym. Advan. Technol.* **2012**, *23*, 1129−1140.
(15) Moniruzzaman, M.; Winey, K. I. *Macromolecules* **2006**, *39*, 5194−5205.
(16) Bachilo, S. M.; Strano, M. S.; Kittrell, C.; Hauge, R. H.; Smalley, R. E.; Weisman, R. B. *Science* **2002**, *298*, 2361−2366.
(17) Iijima, S. *Nature* **1991**, *354*, 56−58.
(18) Tuncel, D. *Nanoscale* **2011**, *3*, 3545−3554.
(19) Star, A.; Stoddart, J. F.; Steuerman, D.; Diehl, M.; Boukai, A.; Wong, E. W.; Yang, X.; Chung, S.; Choi, H.; Heath, J. R. *Angew. Chem., Int. Ed.* **2001**, *40*, 1721−1725.
(20) Dalton, A. B.; Stephan, C.; Coleman, J. N.; McCarthy, B.; Ajayan, P. M.; Lefrant, S.; Bernier, P.; Blau, W. J.; Byrne, H. J. *J. Phys. Chem. B* **2000**, *104*, 10012−10016.
(21) Chen, J.; Liu, H.; Weimer, W. A.; Halls, M. D.; Waldeck, D. H.; Walker, G. C. *J. Am. Chem. Soc.* **2002**, *124*, 9034−9035.
(22) Ferguson, A. J.; Blackburn, J. L.; Holt, J. M.; Kopidakis, N.; Tenent, R. C.; Barnes, T. M.; Heben, M. J.; Rumbles, G. *J. Phys. Chem. Lett.* **2010**, *1*, 2406−2411.
(23) Ren, S.; Bernardi, M.; Lunt, R. R.; Bulovic, V.; Grossman, J. C.; Gradečak, S. *Nano Lett.* **2011**, *11*, 5316−5321.
(24) Cheng, F.; Imin, P.; Maunders, C.; Botton, G.; Adronov, A. *Macromolecules* **2008**, *41*, 2304−2308.
(25) Lu, R.; Christianson, C.; Kirkeminde, A.; Ren, S.; Wu, J. *Nano Lett.* **2012**, *12*, 6244−6249.
(26) Chen, F.; Zhang, W.; Jia, M.; Wei, L.; Fan, X.; Kuo, J.; Chen, Y.; Chan-Park, M. B.; Xia, A.; Li, L. *J. Phys. Chem. C.* **2009**, *113*, 14946−14952.
(27) Chen, F.; Wang, B.; Chen, Y.; Li, L. *Nano Lett.* **2007**, *7*, 3013−3017.
(28) Nish, A.; Hwang, J.; Doig, J.; Nicholas, R. J. *Nature Nanotechnol.* **2007**, *2*, 640−646.
(29) Lemasson, F. A.; Strunk, T.; Gerstel, P.; Hennrich, F.; Lebedkin, S.; Barner-Kowollik, C.; Wenzel, W.; Kappes, M. M.; Mayor, M. *J. Am. Chem. Soc.* **2010**, *133*, 652−655.
(30) Rice, N. A.; Adronov, A. *Macromolecules* **2013**, *46*, 3850−3860.
(31) Lam, J. W. Y.; Tang, B. Z. *Acc. Chem. Res.* **2005**, *38*, 745−754.
(32) Liu, J. Z.; Lam, J. W. Y.; Tang, B. Z. *Chem. Rev.* **2009**, *109*, 5799−5867.
(33) Tang, B. Z.; Xu, H. *Macromolecules* **1999**, *32*, 2569−2576.
(34) Sun, J. Z.; Qin, A.; Tang, B. Z. *Polym. Chem.* **2013**, *4*, 211−223.
(35) Zhao, H.; Yuan, W. Z.; Tang, L.; Sun, J. Z.; Xu, H.; Qin, A.; Mao, Y.; Jin, J. K.; Tang, B. Z. *Macromolecules* **2008**, *41*, 8566−8574.
(36) Zhao, H.; Yuan, W. Z.; Mei, J.; Tang, L.; Liu, X. Q.; Yan, J. M.; Shen, X. Y.; Sun, J. Z.; Qin, A.; Tang, B. Z. *J. Polym. Sci., Part A: Polym. Chem.* **2009**, *47*, 4995−5005.
(37) Yuan, W. Z.; Sun, J. Z.; Liu, J. Z.; Dong, Y.; Li, Z.; Xu, H. P.; Qin, A.; Häussler, M.; Jin, J. K.; Zheng, Q.; Tang, B. Z. *J. Phys. Chem. B* **2008**, *112*, 8896−8905.
(38) Yuan, W. Z.; Sun, J. Z.; Dong, Y.; Häussler, M.; Yang, F.; Xu, H. P.; Qin, A.; Lam, J. W. Y.; Zheng, Q.; Tang, B. Z. *Macromolecules* **2006**, *39*, 8011−8020.
(39) Zheng, J. F.; Liu, X.; Chen, X. F.; Ren, X. K.; Yang, S.; Chen, E. Q. *ACS Macro Lett.* **2012**, *1*, 641−645.
(40) Liu, L. M.; Liu, K. P.; Dong, Y. P.; Chen, E. Q.; Tang, B. Z. *Macromolecules* **2010**, *43*, 6014−6023.
(41) Masuda, T. *J. Polym. Sci., Part A: Polym. Chem.* **2007**, *45*, 165−180.
(42) Xu, K.; Peng, H.; Lam, J. W. Y.; Poon, T. W. H.; Dong, Y.; Xu, H.; Sun, Q.; Cheuk, K. K. L.; Salhi, F.; Lee, P. P. S.; Tang, B. Z. *Macromolecules* **2000**, *33*, 6918−6924.
(43) Tang, B. Z.; Kong, X.; Wan, X.; Feng, X. *Macromolecules* **1997**, *30*, 5620−5628.
(44) Tang, B. Z.; Kong, X.; Wan, X.; Peng, H.; Lam, W. Y.; Feng, X.; Kwok, H. S. *Macromolecules* **1998**, *31*, 2419−2432.
(45) Yang, J.; Yang, N.; Zhang, D.; Wang, X.; Li, Y.; Li, Y. *J. Phys. Chem. C.* **2012**, *116*, 22028−22035.
(46) Strano, M. S.; Dyke, C. A.; Usrey, M. L.; Barone, P. W.; Allen, M. J.; Shan, H.; Kittrell, C.; Hauge, R. H.; Tour, J. M.; Smalley, R. E. *Science* **2003**, *301*, 1519−1522.
(47) Tan, Y.; Resasco, D. E. *J. Phys. Chem. B* **2005**, *109*, 14454−14460.
(48) Imin, P.; Imit, M.; Adronov, A. *Macromolecules* **2011**, *44*, 9138−9145.
(49) Hwang, J.; Nish, A.; Doig, J.; Douven, S.; Chen, C.; Chen, L.; Nicholas, R. J. *J. Am. Chem. Soc.* **2008**, *130*, 3543−3553.
(50) Ohno, Y.; Iwasaki, S.; Murakami, Y.; Kishimoto, S.; Maruyama, S.; Mizutani, T. *Phys. Status Solidi B* **2007**, *244*, 4002−4005.
(51) Stranks, S. D.; Yong, C.; Alexander-Webber, J. A.; Weisspfennig, C.; Johnston, M. B.; Herz, L. M.; Nicholas, R. J. *ACS Nano* **2012**, *6*, 6058−6066.
(52) Attal, S.; Thiruvengadathan, R.; Regev, O. *Anal. Chem.* **2006**, *78*, 8098−8104.
(53) Tian, L.; Meziani, M. J.; Lu, F.; Kong, C. Y.; Cao, L.; Thorne, T. J.; Sun, Y. *ACS Appl. Mater. Interfaces* **2010**, *2*, 3217−3222.
(54) Itkis, M. E.; Perea, D. E.; Niyogi, S.; Rickard, S. M.; Hamon, M. A.; Hu, H.; Zhao, B.; Haddon, R. C. *Nano Lett.* **2003**, *3*, 309−314.
(55) Zhao, B.; Itkis, M. E.; Niyogi, S.; Hu, H.; Zhang, J.; Haddon, R. C. *J. Phys. Chem. B* **2004**, *108*, 8136−8141.
(56) Oyama, Y.; Saito, R.; Sato, K.; Jiang, J.; Samsonidze, G. G.; Grüneis, A.; Miyauchi, Y.; Maruyama, S.; Jorio, A.; Dresselhaus, G.; Dresselhaus, M. S. *Carbon* **2006**, *44*, 873−879.
(57) Lordi, V.; Yao, N. *J. Mater. Res.* **2000**, *15*, 2770−2779.
(58) Jakubka, F.; Schießl, S. P.; Martin, S.; Englert, J. M.; Hauke, F.; Hirsch, A.; Zaumseil, J. *ACS Macro Lett.* **2012**, *1*, 815−819.
(59) Levitsky, I. A.; Euler, W. B. *Appl. Phys. Lett.* **2003**, *83*, 1857−1859.
(60) Itkis, M. E.; Borondics, F.; Yu, A.; Haddon, R. C. *Science* **2006**, *312*, 413−416.
(61) Pradhan, B.; Setyowati, K.; Liu, H.; Waldeck, D. H.; Chen, J. *Nano Lett.* **2008**, *8*, 1142−1146.
(62) Pradhan, B.; Kohlmeyer, R. R.; Setyowati, K.; Owen, H. A.; Chen, J. *Carbon* **2009**, *47*, 1686−1692.